Cell Cycle 14:12, 1809–1822; June 15, 2015; Published with license by Taylor & Francis Group, LLC

FANCD2 influences replication fork processes and genome stability in response to clustered DSBs

Jiayun Zhu[1], Fengtao Su[1], Shibani Mukherjee[2], Eiichiro Mori[1], Burong Hu[3], and Aroumougame Asaithamby[1,*]

[1]Department of Radiation Oncology; Dallas, TX USA; [2]Department of Psychiatry; University of Texas Southwestern Medical Center; Dallas, TX USA; [3]Department of Space Radiobiology; Key Laboratory of Heavy Ion Radiation Biology and Medicine; Institute of Modern Physics; Chinese Academy of Sciences; Lanzhou, PR China

Keywords: clustered DSBs, DNA replication, FANCD2, genome instability, high-LET radiation

Fanconi Anemia (FA) is a cancer predisposition syndrome and the factors defective in FA are involved in DNA replication, DNA damage repair and tumor suppression. Here, we show that FANCD2 is critical for genome stability maintenance in response to high-linear energy transfer (LET) radiation. We found that FANCD2 is monoubiquitinated and recruited to the sites of clustered DNA double-stranded breaks (DSBs) specifically in S/G2 cells after high-LET radiation. Further, FANCD2 facilitated the repair of clustered DSBs in S/G2 cells and proper progression of S-phase. Furthermore, lack of FANCD2 led to a reduced rate of replication fork progression and elevated levels of both replication fork stalling and new origin firing in response to high-LET radiation. Mechanistically, FANCD2 is required for correct recruitment of RPA2 and Rad51 to the sites of clustered DSBs and that is critical for proper processing of clustered DSBs. Significantly, FANCD2-decifient cells exhibited defective chromosome segregation, elevated levels of chromosomal aberrations, and anchorage-independent growth in response to high-LET radiation. These findings establish FANCD2 as a key factor in genome stability maintenance in response to high-LET radiation and as a promising target to improve cancer therapy.

Introduction

If DNA damage induced by ionizing radiation (IR) is not efficiently and accurately repaired, it usually results in cell death or chromosomal aberrations, loss of genome integrity, and carcinogenesis. High-linear energy transfer (LET) radiation, such as high-charge and energy (HZE) particles, is known to produce high levels of clustered DNA damage,[1-3] and that include 2 or more individual lesions within one or 2 helical turns of the DNA by a single radiation track.[4] The 2 basic clustered DNA lesions are double-strand breaks (DSBs) and non-DSBs. The lesions within the clustered DNA lesion can be abasic sites, damage bases (oxidized purines or pyrimidines), single-strand breaks and DSBs.[5,6] The clustered DSBs can be a mixture of DSBs, modified bases and single-strand breaks. Track structure simulations suggest that a majority of DSBs induced by high-LET radiation are associated with other lesions.[7] However, the molecular mechanism by which cells repair clustered DSBs is still elusive.

There are 2 major pathways to repair DSBs in human cells, non-homologous end-joining (NHEJ) and homologous recombination (HR) repair. NHEJ and HR pathways coordinate but function differentially in response to different types of DNA lesions and in different cell cycle phases. Due to the production of small DNA fragments (<40 bp) in cells exposed to high-LET IR, the affinity of Ku, a key NHEJ factor, for the damaged DNA is decreased, and these short fragments of damaged DNA leads to reduced efficiency of NHEJ-mediated clustered DSB repair.[8,9] Evidence suggests that the HR-mediated DSB repair pathway is partially involved in repairing clustered DSBs.[10] The complexity of DNA damage also appears to be a critical factor in facilitating DNA end-resection,[11] a crucial step in HR repair. Thus, these data suggest that a single DNA repair pathway may not able to deal with the clustered DNA lesions and their repair requires coordinated and sequential activities of factors belonging to different DNA metabolic pathways.

The Fanconi Anemia (FA) is a rare inherited syndrome that is characterized by congenital abnormalities, progressive bone marrow failure, and a highly elevated risk of hematological and squamous cell cancer.[12] FA is a genetically heterogeneous disease, with 16 complementation groups identified to date.[13-16] A central event in the FA pathway is the monoubiquitination of FANCD2 and FANCI upon DNA damage; this modification is mediated by the FA core complex, consisting of 8 proteins (FANCA, B, C, E, F, G, L and M).[17,18] Upon ubiquitination, FANCD2 and FANCI heterodimerize and functionally interact with downstream FA proteins such

*Correspondence to: Aroumougame Asaithamby; Email: Asaithamby.Aroumougame@UTsouthwestern.edu
Submitted: 03/03/2015; Revised: 03/12/2015; Accepted: 03/26/2015
http://dx.doi.org/10.1080/15384101.2015.1036210

as FANCD1/BRCA2, FANCN/PALB2, FANCJ/BRIP1, FANCP/SLX4, RAD51C, and their associated protein, BRCA1.[13-15,19] Additionally, chemical inhibition of FANCD2 sensitizes certain types of cancer to chemotherapy,[20,21] implying the significance of FA pathway in tumor suppression.

FANCD2 plays roles in replication, recombination, repair, and recovery in response to a variety of DNA damaging agents. The monoubiquitinated FANCD2 co-localizes with HR repair pathway factors such as BRCA1 and Rad51.[22] Further, the basal level of FANCD2 monoubiquitination is required for the maintenance of a sufficient number of licensed-replication origins to fire at a normal rate.[23] FANCD2 also interacts with CtIP to regulate DNA-end resection during DNA repair.[24,25] FANCD2 is clearly important in interstrand cross-link repair and have additional roles in replication fork maintenance[26] and in the S-phase checkpoint.[27] As a single DNA repair pathway may not be sufficient to deal with clustered DSBs, it is possible that FANCD2 may coordinate the functions of multiple DNA metabolic factors in response to clustered DNA lesions induced by high-LET radiation.

Here, we show that FANCD2 is monoubiquitinated in response to high-LET Fe-particles radiation and is recruited to the sites of clustered DSBs specifically in S/G2 cells. Further, FANCD2 modulates proper recruitment of RPA2 and Rad51 to the sites of clustered DSBs and is critical for the repair of clustered DSBs in S/G2 cells. Furthermore, FANCD2 functions during S-phase progression and replication fork processes in response to Fe-particles radiation. Importantly, all these coordinated functions of FANCD2 are crucial for the suppression of genomic instability in human cells. Thus, our study reveals a previously unidentified role for FANCD2 in the suppression of genome instability in response to high-LET radiation.

Results

FANCD2 is activated in S/G2 cells in response to high-LET iron-particles radiation

The monoubiquitination of FANCD2 is a critical step in the activation of the FA pathway in response to DNA damage.[17,18] Therefore, first we verified whether FANCD2 is monoubiquitinated in response to Fe-particles radiation. As shown in **Figure 1A**, FANCD2 was weakly monoubiquitinated in mock-treated HT1080 cells. The level of FANCD2 monoubiquitination gradually increased with time after exposure of HT1080 cells to 2 Gy Fe-particles and reached the maximum level at 8 hours after Fe-particles radiation. Thus, similar to low-LET IR,[17] FANCD2 is monoubiquitinated in response to high-LET Fe-particles radiation.

Evidence suggests that monoubiquitination of FANCD2 is required for its localization to damaged DNA.[17] To examine whether FANCD2 is recruited to the sites of clustered DSBs induced by Fe-particles radiation, we exposed FANCD2$^{-/-}$ cells complemented with FANCD2 to Fe-particles and immunostained with anti-FANCD2 and anti-γH2AX. As shown in **Figure 1B**, FANCD2 formed distinct foci along the densely ionizing tracks traversed by Fe-particles, and the FANCD2 foci were detected as early as 30 min after Fe-particles irradiation. Interestingly, unlike γH2AX, FANCD2 formed foci only in a subset of cells in response to Fe-particles irradiation (**Fig. S1**). To verify the type of cells that formed FANCD2 foci, we used a newly generated HT1080 cell line, HT1080-FUCCI cells[28] that express different fluorescent markers depending on the phase of the cell cycle: G1 cells are red, early S are yellow, and S/G2 are green. We irradiated exponentially growing HT1080-FUCCI cells with 2 Gy of Fe-particles and examined the recruitment of FANCD2 by indirect immunostaining using anti-FANCD2. We observed distinct FANCD2 foci along the tracks of Fe-particles only in S/G2 cells (**Fig. 1C**). Further, a majority of the FANCD2 foci clearly co-localized with γH2AX foci. Thus, these results reveal that recruitment of FANCD2 to the sites of clustered DSBs is restricted to S/G2 phases of the cell cycle.

FANCD2 contributes to the repair of clustered DNA damage in S/G2 cells

Next, we evaluated whether FANCD2 is important for cellular sensitivity to Fe-particles radiation using a colony formation assay. In general, cells were more sensitive to Fe-particles than to γ-irradiation (**Fig. 2A**). Similar to a previous report,[29] FANCD2$^{-/-}$ cells were slightly more sensitive to γ-irradiation than were the FANCD2-WT cells. Similarly, FANCD2$^{-/-}$ cells were slightly more sensitive to Fe-particles irradiation than the FANCD2-WT cells (**Fig. 2A**). The calculated relative biological effectiveness values at 10% cell survival for FANCD2-WT and FANCD2$^{-/-}$ cells irradiated with Fe-particles relative to γ-rays were 3.04 and 3.74, respectively. These results imply that FANCD2 plays a role in cellular sensitivity to Fe-particles radiation.

To determine whether the recruitment of FANCD2 to the sites of clustered DSBs is important for the repair of clustered DSBs, we enumerated γH2AX foci dissolution kinetics in FANCD2-WT and FANCD2$^{-/-}$ cells at different times after Fe-particles exposure (**Fig. 2B**). As shown in **Figure 2C**, the γH2AX foci dissolution kinetics were slower in FANCD2$^{-/-}$ cells than in FANCD2-WT cells. Further, the number of persistent γH2AX foci was significantly higher in Fe-irradiated FANCD2$^{-/-}$ cells (8.7 ± 0.5 foci per cell) than in FANCD2-WT cells exposed to Fe-particles (3.6 ± 0.3 foci per cell; $P = 0.02$). The higher number of residual γH2AX foci in FANCD2$^{-/-}$ cells suggests that FANCD2 is involved in the processing of clustered DSBs.

Since recruitment of FANCD2 to the sites of clustered DSBs was restricted to S/G2 phases, it is possible that the unrepaired DSBs are only present in FANCD2$^{-/-}$ cells in the S/G2 phase of the cell cycle. To verify this, we pulse-labeled cells with ethyldeoxyuridine (EdU) and immediately exposed cells to Fe-particles. The cells labeled with EdU are those in S-phase at the time of irradiation. We detected γH2AX foci in EdU-positive and EdU-negative FANCD2-WT and FANCD2$^{-/-}$ cells at different post-IR times (**Fig. 2D**). The levels of γH2AX foci were indistinguishable between EdU-negative FANCD2-WT and EdU-negative FANCD2$^{-/-}$ cells at 24 hours after IR (**Fig. 2E**). In contrast, a majority of the EdU-positive FANCD2$^{-/-}$ cells (90 ± 2%)

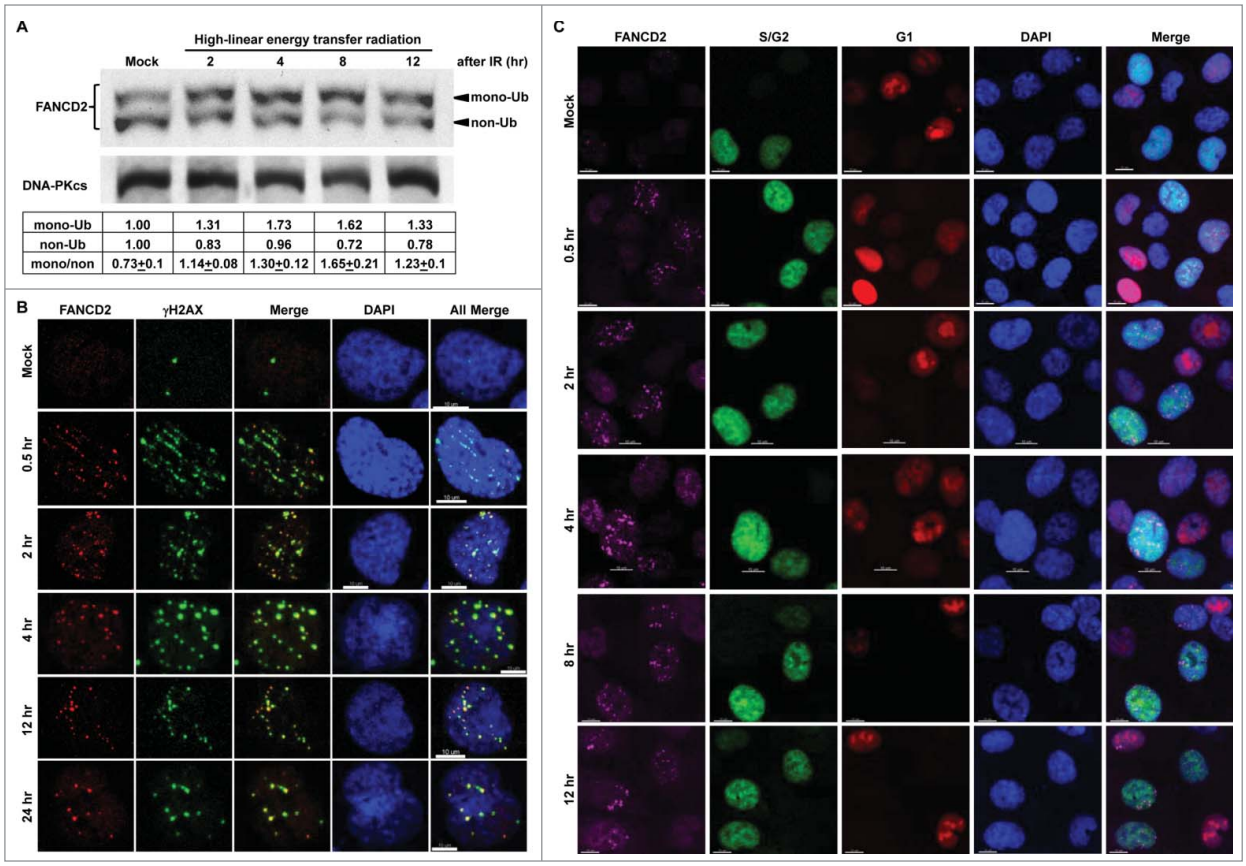

Figure 1. FANCD2 is recruited to the sites of clustered DSBs in S/G2 cells in response to high-LET radiation. (**A**) FANCD2 is monoubiquitinated in response to iron (Fe)-particles radiation: Western blot shows monoubiquitylation of FANCD2 after Fe-particles. Exponentially growing HT1080 cells were exposed to 2 Gy of Fe-particles and were harvested at indicated times after Fe-particles radiation. Approximately 100 μg of total cell lysate was separated on a 6% SDS-PAGE, and blots were probed with anti-FANCD2. Anti-DNA-PKcs was used as a loading control. The signal intensity was quantified in 2 independent experiments using ImageJ. (**B**) FANCD2 is recruited to the sites of clustered DSBs: FANCD2$^{-/-}$ cells stably expressing FANCD2 were exposed to 2 Gy of Fe-particles and fixed at indicated times after Fe-particles radiation. Cells were immunostained with anti-FANCD2 and anti-γH2AX and were imaged using a confocal microscope. Representative confocal images are shown. Scale bars are 10 μm. (**C**) FANCD2 is recruited to the sites of clustered DSBs only in S/G2 cells: HT1080 cells stably expressing 2 different cell cycle markers, mCherry (G1) and AmCyan (S/G2), were exposed to 2 Gy of Fe-particles, and immunostained with anti-FANCD2 at indicated times after Fe-particles radiation. Cells were imaged using a confocal microscope. Red, red/green, and green fluorescent cells represent G1, early S, and S/G2 phases, respectively. Representative confocal images are shown. Scale bars are 10 μm.

retained a significantly higher number of γH2AX foci as compared with EdU-positive FANCD2-WT cells (1.5 ± 0.3 and 6.7 ± 1.27 foci per cell in FANCD2-WT and FANCD2$^{-/-}$ cells, respectively; $p = 0.03$; **Fig. 2F**). These results suggest that S/G2 FANCD2$^{-/-}$ cells cannot fully repair clustered DSBs.

Dynamics of RPA2 and RAD51 at the sites of clustered DSBs are defective in Fe-particles irradiated FANCD2$^{-/-}$ cells

We next sought to determine why FANCD2$^{-/-}$ cells cannot efficiently repair clustered DSBs. Evidence suggests that the HR pathway is required for the repair of clustered DNA damage,[10] and FANCD2 participates in HR-mediated repair.[22,30–32] Therefore, we reasoned that FANCD2 might collaborate with HR pathway factors in the processing of clustered DSBs. To verify this idea, first we examined whether FANCD2 co-localizes with Rad52, an HR factor,[33,34] after Fe-particles radiation. We irradiated U2OS cells stably expressing mCherry-Rad52 and a cyan S/G2 marker with Fe-particles and immunostained with anti-FANCD2. As shown in **Figures 3A and S2**, FANCD2 clearly co-localized with Rad52 only in S/G2 cells after Fe-particles irradiation. Thus, FANCD2 may collaborate with HR pathway factors in repairing clustered DSBs.

A major step in HR repair is DNA-end resection.[35] Evidence suggests that DNA-end resection is important for the repair of clustered DSBs.[11,36] Recent reports indicate that FANCD2 interacts with CtIP, a factor critical for DNA-end resection.[24,25] Therefore, we hypothesized that lack of FANCD2 results in defective DNA-end resection and inefficient repair of clustered DSBs. Hence, we evaluated the extent of DNA-end resection using RPA2 foci as a surrogate marker. The number of RPA2 foci increased gradually in Fe-particles irradiated FANCD2-WT cells and reached maximum levels between 8 and 12 hours after IR (**Fig. 3B and C**). In contrast,

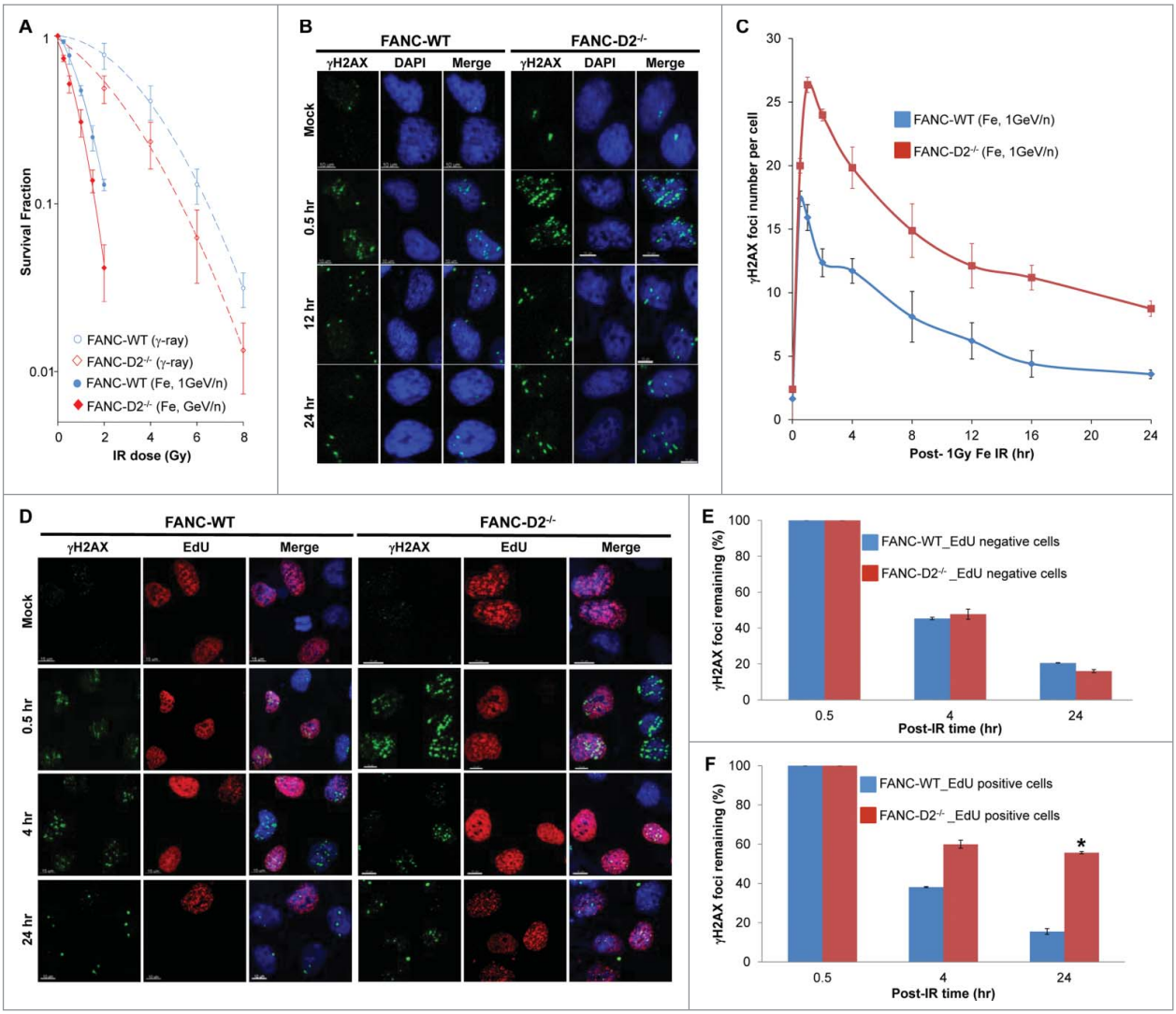

Figure 2. FANCD2 is important for the repair of clustered DSBs in S/G2 cells. (**A**) FANCD2$^{-/-}$ cells are moderately sensitive to Fe-particles radiation: FANCD2-WT and FANCD2$^{-/-}$ cells were exposed to graded doses of γ-rays and high-LET Fe-particles and then subjected to a colony formation assay. Colonies were fixed and counted. The relative survival efficiencies are plotted. The error bars represent the STDEV calculated from 4 independent experiments. (**B, C**) FANCD2-deficient cells are defective in clustered DSBs repair: Representative confocal images show different levels of γH2AX foci at indicated times after Fe-particles radiation (**B**). Graph shows quantification of γH2AX foci in FANCD2-WT and FANC-D2$^{-/-}$ cells exposed to 1Gy of Fe-particles (**C**). Cells were fixed with 4% PFA at indicated times after Fe-particles radiation, immunostained with anti-γH2AX and the number of γH2AX foci was enumerated using Imaris software (Bitplane). The number of γH2AX foci in 150–200 cells was counted for each time point. Error bars represent STDEV calculated from 3 independent experiments. (**D–F**) Unrepaired clustered DSBs persist in S/G2 FANCD2$^{-/-}$ cells: Representative confocal images show γH2AX foci in EdU-positive (S/G2) and EdU-negative (G1) cells (**D**). Graphs show quantification of γH2AX foci in EdU-negative (**E**) and EdU-positive cells (**F**). Cells were labeled with EdU for 30 min and then immediately exposed to 1Gy of Fe-particles. Cells were fixed at 0.5, 4, and 24 hours after irradiation, and images were acquired using confocal microscopy. The γH2AX foci in EdU-positive (G1) and negative (S/G2) cells were enumerated using Imaris Software (Bitplane). The average number of foci at the 30-min time point was taken as 100%. Error bars represent STDEV calculated from 2 independent experiments.

the number of RPA2 foci was significantly lower in Fe-particles exposed FANCD2$^{-/-}$ cells than in Fe-particles irradiated FANCD2-WT cells ($p = 0.01$ and $p = 0.006$ at 8 and 12 hours, respectively). These results imply that end-resection, as marked by RPA2, is defective in FANCD2$^{-/-}$ cells. We next evaluated Rad51 nucleofilament formation. The extent of Rad51 nucleofilament formation at the sites of DNA damage differed in FANCD2-WT and FANCD2$^{-/-}$ cells (**Fig. 3B and D**). There were fewer Rad51 foci in Fe-particles irradiated FANCD2$^{-/-}$ cells than in Fe-particles-treated FANCD2-WT cells (**Fig. 3D**). Thus, these results provide evidence that in the absence of FANCD2 formation of RPA2 foci and Rad51 nucleofilaments are reduced, likely contributing to the inefficient repair of clustered DSBs in FANCD2$^{-/-}$ cells.

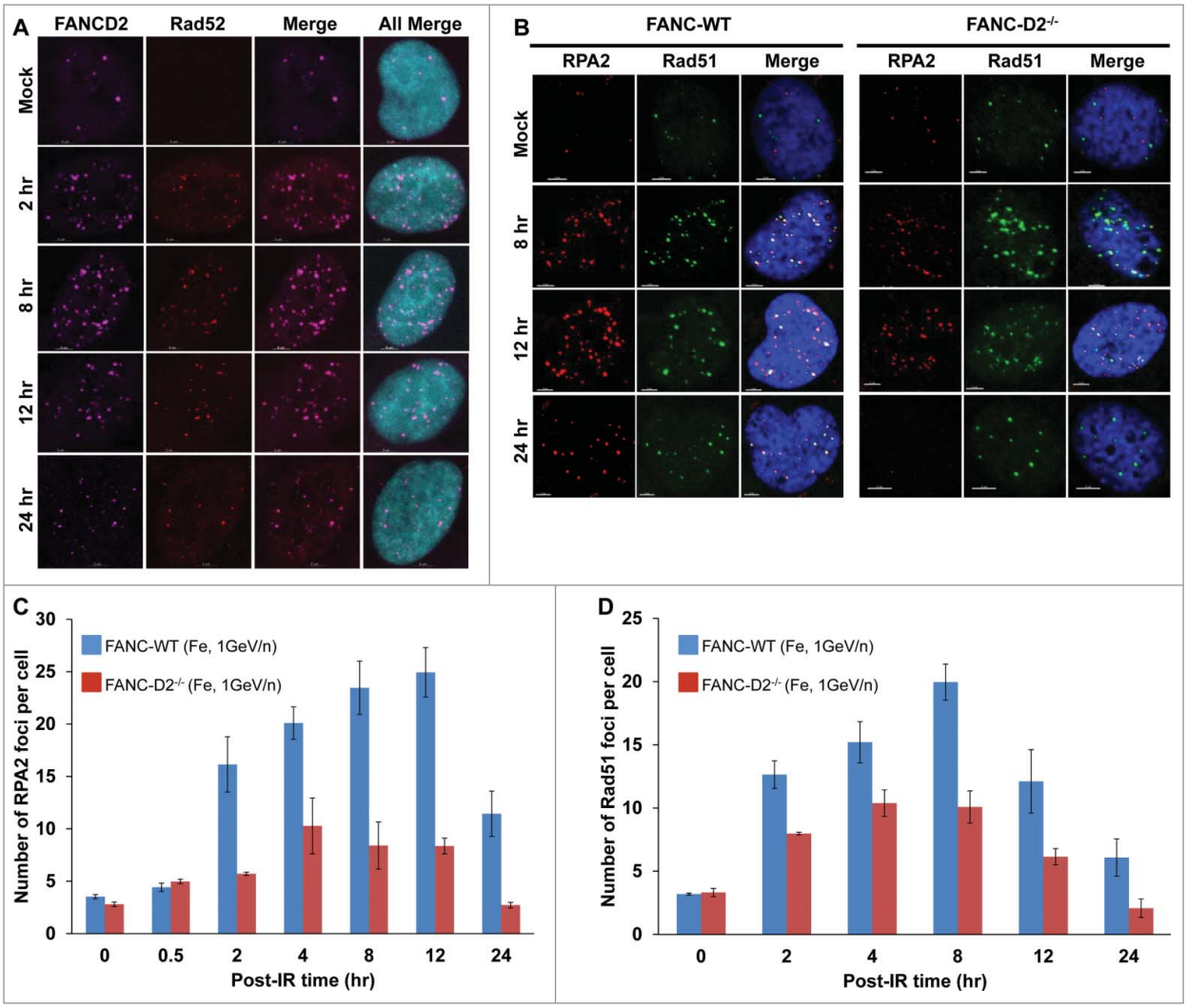

Figure 3. Recruitment of RPA2 and RAD51 are defective in FANCD2$^{-/-}$ cells after Fe-particles radiation. (**A**) FANCD2 co-localizes with Rad52 in S/G2 cells in response to Fe-particles radiation: Representative images show co-localization of FANCD2 with Rad52 in S/G2 cells in response to Fe-particles radiation. Exponentially growing U2OS cells stably expressing the AmCyan-S/G2 marker and mCherry-Rad52 were exposed to 1 Gy of Fe-particles and immunostained with anti-FANCD2 at indicated times after IR. Images were acquired using a confocal microscope. Scale bars are 5 μm. (**B–D**) Recruitment of RPA2 and RAD51 are attenuated in Fe-particles treated FANCD2$^{-/-}$ cells: Representative images show recruitment and retention of RPA2 and Rad51 foci at clustered DSBs in FANCD2-WT and FANCD2$^{-/-}$ cells (**B**). Graphs show number of RPA2 (**C**) and Rad51 (**D**) foci in FANC-WT and FANC-D2$^{-/-}$ cells. Cells were exposed to 1 Gy of Fe-particles, fixed with 4% PFA at indicated times after IR and immunostained with anti-RPA2 and anti-Rad51. The RPA2 and Rad51 foci in 150–200 cells were counted for each time point. Error bars represent STDEV calculated from 3 independent experiments. Scale bars are 5 μm.

FANCD2 functions in replication forks maintenance in response to Fe-particles radiation

FANCD2 has been implicated in replication fork progression and efficient restart in response to replication stress.[37] To verify the role of FANCD2 in replication fork processes in response to Fe-particles radiation, we evaluated replication fork progression, stalling, and origin firing using a single-molecule DNA fiber technique.[38] Examination of replication fork progression showed that the replication fork lengths (determined using IdU-labeling) were identical between mock-treated FANCD2-WT and FANCD2$^{-/-}$ cells (5.14 ± 0.01 and 5.15 ± 0.06 in FANCD2-WT and FANCD2$^{-/-}$ cells, respectively, **Fig. 4A**). In contrast, replication fork lengths (labeled with CIdU) in Fe-particles exposed FANCD2$^{-/-}$ cells were shorter than those in irradiated FANCD2-WT cells (4.32 ± 0.06 and 3.29 ± 0.05 in FANCD2-WT and FANCD2$^{-/-}$ cells, respectively; $P < 0.003$, **Fig 4B**). Thus, these results imply that FANCD2 is important for normal replication fork progression in response to Fe-particles radiation.

Subsequently, we evaluated the extent of replication fork restart, stalling, and new origin firing in Fe-particles irradiated cells by sequential labeling of replicating DNA with IdU and CldU before and after Fe-particles radiation, respectively.

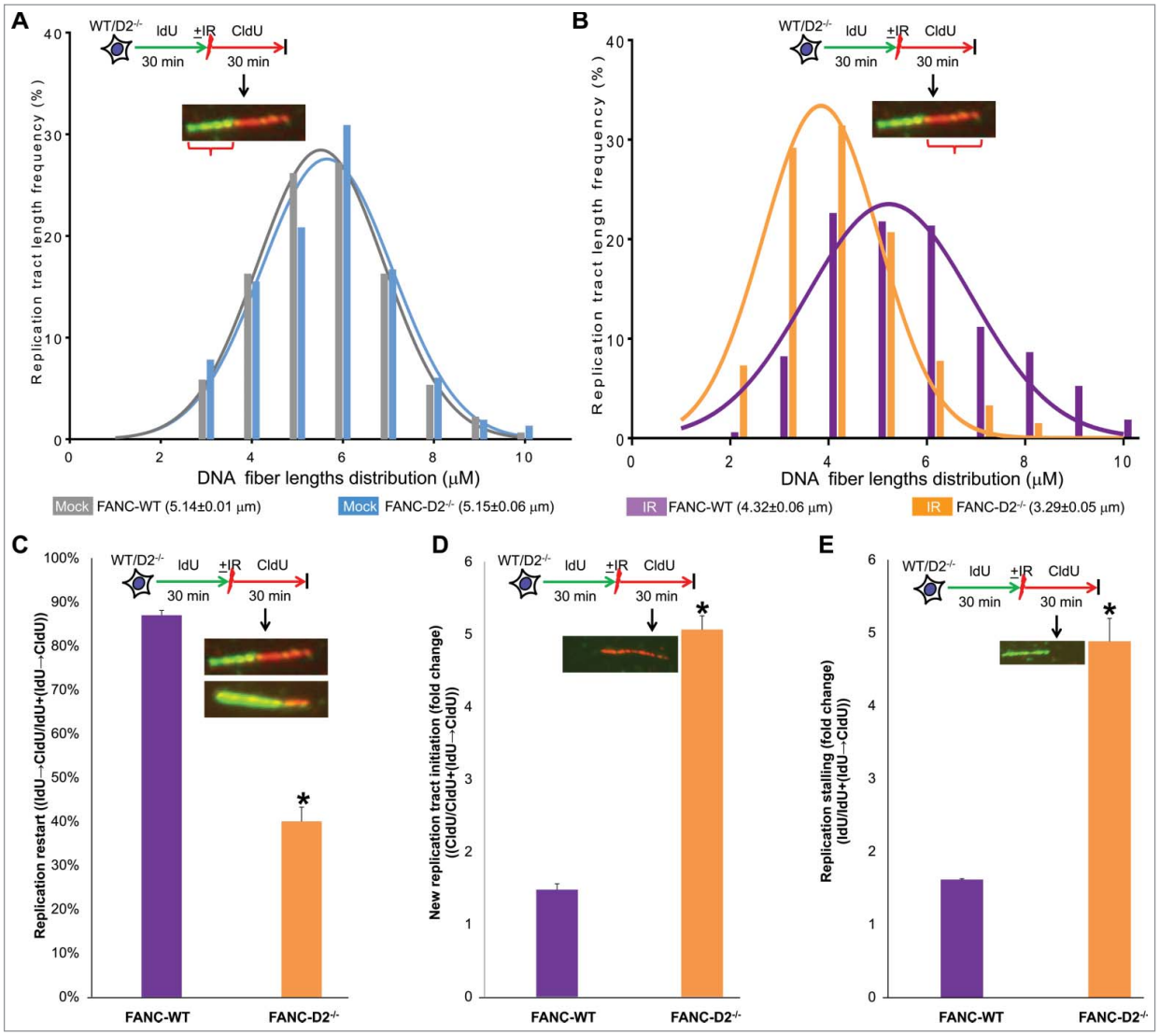

Figure 4. FANCD2 is critical for proper DNA replication processes in response to Fe-particles radiation. (**A, B**) Replication fork progression is reduced in FANCD2$^{-/-}$ cells in response to Fe-particles radiation: The graph shows DNA fiber length distributions in FANC-WT and FANC-D2$^{-/-}$ cells prior to Fe-particles exposure (**A**). The graph shows DNA fiber length distributions in FANCD2-WT and FANCD2$^{-/-}$ cells after Fe-particles irradiation (**B**). Cells were labeled with IdU for 30 min, treated with ± Fe-particles (1Gy) and then labeled with CldU for another 30 min. DNA fibers were immunostained with anti-BrdU (rat and mouse), images were captured using a fluorescence microscopy, and DNA fiber lengths were measured using Axiovison Software. More than 200 DNA fibers were evaluated in each sample. Each data point is the average of 2 or 3 independent experiments. (**C–E**) Replication forks stall in FANCD2$^{-/-}$ cells in response to Fe-particles radiation: The graph shows percentages of replication fork restarts in Fe-particles irradiated FANCD2-WT and FANCD2$^{-/-}$ cells relative to mock-treated cells was evaluated using the {(IdU→CldU)/[IdU+(IdU→CldU)]} formula (**C**). The graph shows fold changes in new origin firing in Fe-particle radiated FANCD2-WT and FANCD2$^{-/-}$ cells relative to mock-treated cells were calculated using the {CldU/[CldU+(IdU→CldU)]} formula (**D**). The graph shows fold changes in replication forks stalling in FANCD2-WT and FANCD2$^{-/-}$ cells relative to mock-irradiated cells were evaluated using the {IdU/[IdU+(IdU→CldU)]} formula (**E**). More than 200 DNA fibers in each sample were evaluated. Each data point is the average of 2 independent experiments. Error bars represent STDEV. *-$P < 0.05$.

As shown in **Figure 4C**, 39 ± 5.7% of all DNA fibers had both IdU and CldU tracts in Fe-irradiated FANCD2$^{-/-}$ cells, whereas 87.2 ± 7.8% fibers contained both IdU and CldU in Fe-particles irradiated FANCD2-WT cells (**Fig. 4C**). These results indicate that a greater proportion of replication forks fail to restart in Fe-particles irradiated FANCD2$^{-/-}$ cells than in Fe-particles exposed FANCD2-WT cells. Furthermore, we observed significantly fewer DNA fibers containing only CldU tracts, which represent new origins of replication, in FANCD2$^{-/-}$ cells than in FANCD2-WT cells (1.5 ± 0.1 and 5.1 ± 0.2 fold fewer in FANCD2-WT and FANCD2$^{-/-}$ cells, respectively, relative to mock-treated cells, $P < 0.014$, **Fig. 4D**). Importantly, a significantly higher percentage of DNA fibers contained only IdU tracts, which

represent stalled forks, in Fe-particles exposed FANCD2$^{-/-}$ cells than in Fe-particles irradiated FANCD2-WT cells (1.6 ± 0.3 and 4.9 ± 0.3, FANCD2-WT and FANCD2$^{-/-}$ cells, respectively, $P < 0.034$, **Fig. 4E**). Thus, a greater proportion of replication forks break in Fe-particles exposed FANCD2$^{-/-}$ cells than in Fe-particles-treated FANCD2-WT cells. These results imply that FANCD2 is critical for replication fork restart and suppression of new origin firing in response to Fe-particles radiation.

FANCD2 facilitates S-phase progression in response to Fe-particles radiation

Evidence suggests that FANCD2 is required for intra-S phase checkpoint activation[29] and FANCD2-deficient S/G2 cells showed inefficient clustered DSB repair and defective replication fork processes (**Fig. 2E**). To investigate how these defects impact cell cycle progression, we systematically examined induction and maintenance of G1/S, intra-S, and G2/M checkpoints in FANCD2-WT and FANCD2$^{-/-}$ cells by flow cytometry (**Fig. 5A**). First, we evaluated S-phase progression in FANCD2-WT and FANCD2$^{-/-}$ cells. We pulse-labeled cells with BrdU and immediately irradiated with Fe-particles. The BrdU-labeled cells represent those in S-phase at the time of irradiation, and the progression of BrdU-positive cells through cell cycle was analyzed by flow cytometry at various time points after irradiation. Our flow cytometry data revealed a differential progression to S phase between FANCD2-WT and FANCD2$^{-/-}$ cells (**Fig. 5B**). FANCD2$^{-/-}$ cells were arrested in early S-phase for the first 2–4 hours and then entered into middle S-phase at 4 hour after Fe-particles irradiation (**Fig. 5B**). In contrast, FANCD2-WT cells progressed into middle S-phase without a delay. The early S-phase delay in FANCD2$^{-/-}$ cells was specific to high-LET IR, since no S-phase arrest was detected in FANCD2$^{-/-}$ cells in response to low-LET IR (**Fig. S3**).

Further, the S-phase arrest observed in FANCD2$^{-/-}$ cells was not a permanent arrest, as BrdU-positive cells had progressed to G2 at 4 hours after Fe-IR (**Fig. 5C**). There were no significant differences in the numbers of BrdU-positive cells in G2 phase between FANCD2-WT and FANCD2$^{-/-}$ cells at different times after high-LET IR. Subsequently, we tested the contribution of FANCD2 to the G2/M checkpoint. As previously described for low-LET IR,[29] FANCD2-WT and FANCD2$^{-/-}$ cells showed identical mitotic phase progression in response to high-LET IR (**Fig. 5D**). FANCD2-WT and FANCD2$^{-/-}$ cells were arrested in mitosis during the first 6 hours after Fe-particles radiation. However, cells began to enter into mitosis 6 hours after IR, and the mitotic index returned to the pre-irradiation levels in FANCD2-WT and FANCD2$^{-/-}$ cells at 10 hours after irradiation (**Fig. 5D**). Thus, the G2/M checkpoint is intact in FANCD2-deficient cells in response to clustered DNA damage. Taken together, these results reveal that FANCD2 affects only the S-phase progression in response to Fe-particles radiation but not the G2/M phases of the cell cycle.

FANCD2 suppresses genomic instability in response to clustered DSBs

To investigate whether defective repair of clustered DSBs in FANCD2$^{-/-}$ cells leads to genome instability, we evaluated metaphase cells for gross chromosomal aberrations after exposure to Fe-particles. As shown in **Figure 6A**, the levels of chromosomal aberrations per chromosome were significantly elevated in Fe-particles irradiated FANCD2$^{-/-}$ cells (0.069 ± 0.01; P = 0.008) relative to Fe-particles exposed FANCD2-WT cells (0.048 ± 0.01). Further, Fe-particles exposure resulted in the generation of a spectrum of chromatid and chromosomal aberrations in both FANCD2-WT and FANCD2$^{-/-}$ cells (**Fig. 6B**). However, the levels of tri-radials, chromosomal breaks, and acentrics were significantly higher in FANCD2$^{-/-}$ cells than in FANCD2-WT cells. Thus, these results imply that FANCD2 suppresses chromosomal instability in response to Fe-particles radiation.

A common cause and indicator of chromosomal instability is the formation of anaphase bridges.[39,40] Anaphase bridges are chromatin fibers connecting the 2 separating chromosome masses. These may arise from mis-segregated whole chromosomes or in acentric chromosomal fragments when pulled in opposite directions by the spindle apparatus.[41] A hallmark of failed chromosome segregation is the appearance of DAPI-positive chromosome bridges and lagging chromosomes.[42] We quantified chromosomal bridges in anaphase cells in mock- and Fe-particles irradiated FANCD2-WT and FANCD2$^{-/-}$ cells using acetylated α-tubulin as a cytokinesis marker[43] and the DNA dye DAPI (**Fig. 6C**). We detected DAPI linkages between anaphase chromosomes in Fe-particles irradiated FANCD2-WT and FANCD2$^{-/-}$ cells (**Fig. 6D**). The frequency of anaphase bridges was significantly higher in Fe-particles irradiated FANCD2$^{-/-}$ cells (55.9 ± 3.5; % p = 0.014) than in Fe-particles irradiated FANCD2-WT cells (23.8 ± 1.7%; **Fig. 6D**). These findings indicate that the FANCD2 is critical for chromosome segregation in response to Fe-particles radiation.

Next, we determined whether elevated levels of chromosomal aberrations and lagging chromosomes in high-LET Fe-particles exposed FANCD2$^{-/-}$ cells resulted in cellular transformation. We used a soft agar assay, an extensively used method to define the transformed nature of cells. As shown in **Figure 6E**, Fe-particles irradiated FANCD2$^{-/-}$ cells (5.5 ± 1.6; p = 0.03) formed a significantly higher number of colonies in soft-agar than did the FANCD2-WT cells (1.6 ± 0.3), reflecting a role for FANCD2 in preventing cellular transformation in response to high-LET radiation.

Discussion

To our knowledge, this is the first report that FANCD2 functions in the cellular response to high-LET Fe-particles radiation in human cells. Using a cell line that differentiates cells in different stages of the cell cycle, we found that FANCD2 was recruited to the sites of clustered DSBs only in S/G2 cells. Activated FANCD2 facilitates clustered DSB repair, S phase progression

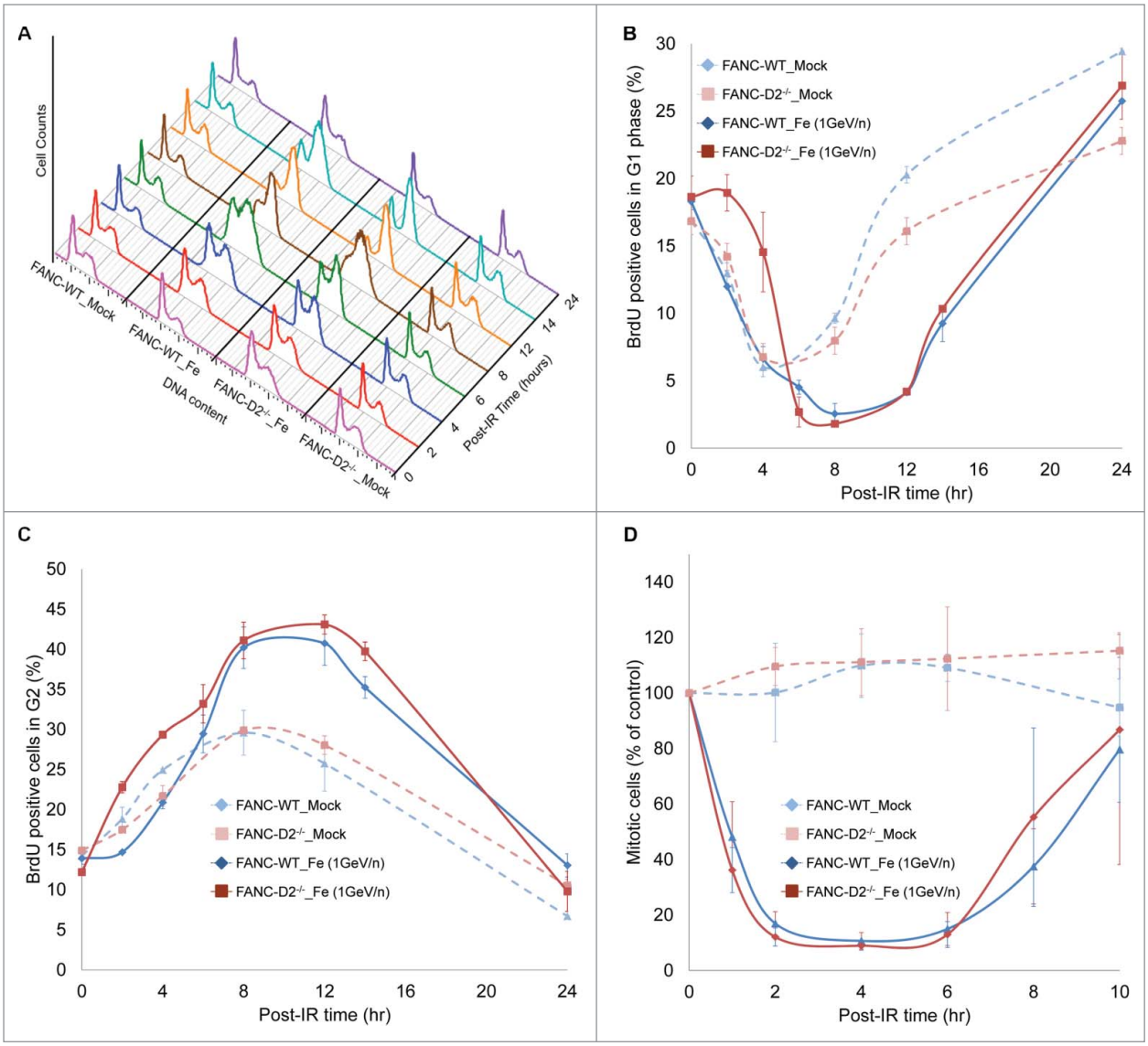

Figure 5. FANCD2 is critical for proper S-phase progression in response to Fe-particles radiation. (**A**) Cell cycle progression is altered in FANCD2$^{-/-}$ cells exposed to Fe-particles: Representative histograms show cell cycle profile at indicated times after mock- or treatment with 1 Gy of Fe-particles. Exponentially growing FANCD2-WT and FANCD2$^{-/-}$ cells were either mock-treated or 1Gy Fe-irradiated, collected at indicated times, and then stained with propidium iodide for DNA content. Subsequently, cells were subjected to single-parameter flow cytometry. More than 20,000 cells in 3 independent experiments were analyzed. (**B, C**) S-phase progression is defective in Fe-particles irradiated FANCD2-deficient cells: The graphs show percentage of BrdU-positive cells in early- (**B**) and late- (**C**) S-phase at indicated times after mock-treatment or irradiation with 1 Gy of Fe-particles. Exponentially growing FANCD2-WT and FANCD2$^{-/-}$ cells were pulse-labeled with BrdU for 30 min and then irradiated with 1 Gy of Fe-particles. Subsequently, cells were immunostained with FITC-conjugated anti-BrdU and then subjected to flow cytometry. More than 20,000 cells in each experiment were analyzed. Error bars represent STDEV calculated from 3 independent experiments. (**D**) G2/M checkpoint is intact in FANCD2-deficient cells in response to Fe-particles radiation: Graph shows percentage of M-phase cells relative to pre-irradiated FANCD2-WT and FANCD2$^{-/-}$ cells at indicated times. Exponentially growing FANCD2-WT and FANCD2$^{-/-}$ cells were either mock-treated or irradiated with 1 Gy of Fe-particles. Subsequently, cells were immunostained with anti-pH3 and subjected to flow cytometry. More than 20,000 cells in each experiment were analyzed. Error bars represent STDEV calculated from 3 independent experiments.

and replication forks processes. By analysis of cells lacking FANCD2, we showed that FANCD2 is involved in the efficient recruitment of RPA2 and Rad51 to the sites of clustered DSBs. Furthermore, lack of FANCD2 resulted in increases in gross chromosomal aberrations, chromosome mis-segregation, and elevated levels of anchorage-independent growth. Thus, FANCD2 orchestrates cellular responses to clustered DSBs, and these activities are critical for maintenance of genomic stability in cells exposed to high-LET radiation.

We found that the number of unrepaired clustered DSBs was higher in Fe-particles irradiated FANCD2$^{-/-}$ cells than in Fe-particles irradiated FANCD2-WT cells. The Ku-dependent

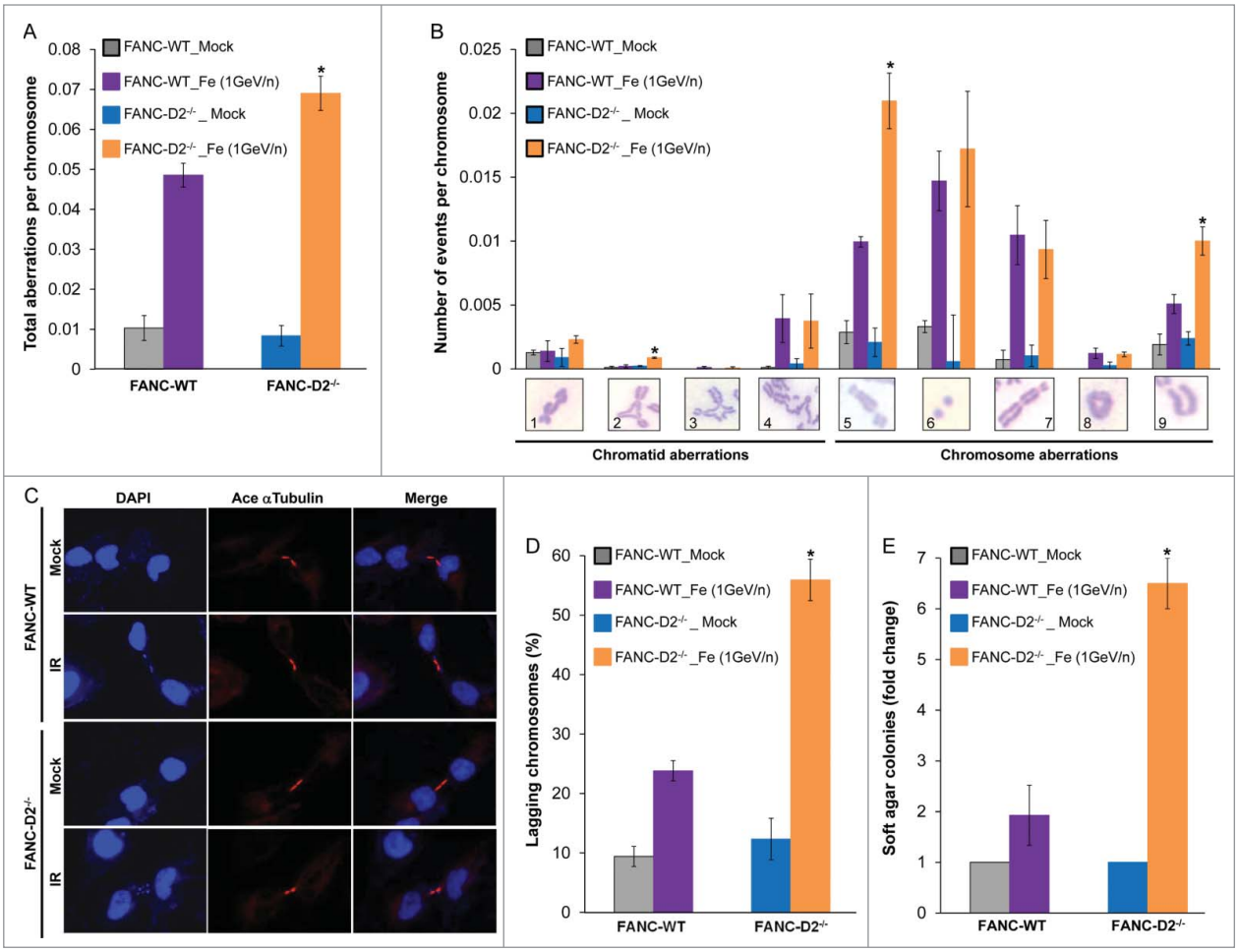

Figure 6. FANCD2 suppresses genome instability in response to Fe-particles radiation. (**A, B**) FANCD2 cells exhibit elevated levels of chromosomal aberrations in response to Fe-particles radiation: Graphs show the levels of gross chromosomal aberrations (**A**) and the distribution of different types of chromosomal aberrations per chromosome (**B**) in mock- and Fe particles-treated FANCD2-WT and FANCD2$^{-/-}$ cells. Exponentially growing cells were either mock-treated or irradiated with 1 Gy of Fe-particles; metaphase chromosomes were prepared 16 hr after IR. Chromosomal aberrations in more than 100 metaphase spreads from 4 independent experiments in each group were scored. Error bars represent STDEV calculated from 4 independent experiments. Key: 1, chromatid break; 2, triradial; 3, quadriradial; 4, interchange; 5, chromosome break; 6, double minutes; 7, dicentric; 8, ring; 9, acentric; *-$P <$ 0.01. (**C, D**) FANCD2 functions in chromosome segregation in response to Fe-particles radiation: Representative images show telophase cells with and without lagging chromosomes in mock- and Fe-particles irradiated FANC-WT and FANC-D2$^{-/-}$ cells (**C**). Graph shows the percentage of lagging chromosomes in mock- and Fe-particles irradiated FANCD2-WT and FANCD2$^{-/-}$ cells (**D**). Cells were exposed to 1 Gy of Fe-particles, immunostained with acetylated α-tubulin at 72 hr after IR and images were acquired using a fluorescent microscope. The percentage of anaphase bridges in more than100 telophases was scored. The error bars represent the STDEV calculated from 2 independent experiments. (**E**) FANCD2 suppresses anchorage-independent growth in response to Fe-particles radiation: Graph shows the fold changes in the frequency of soft-agar colonies formed by Fe-particles irradiated FANCD2-WT and FANCD2$^{-/-}$ cells normalized to corresponding mock-treated samples. Cells were exposed to 2 Gy of Fe-particles and were allowed to form anchorage-independent colonies in soft-agar for 45 days. Colonies were fixed and stained with 1 mg/ml iodonitrotetrazolium violet overnight at 37°C. Fold change was calculated by taking the transformation frequency of mock-treated samples as 1. The transformation ratio was calculated. Error bars represent SEM calculated from 2 independent experiments. *-$P < 0.05$.

NHEJ pathway is not required for the repair of high-LET radiation-induced clustered DSBs,[44] but the HR pathway is.[10] As shown previously, FANCD2 co-localizes with HR factors Rad51[22] and Rad52 (**Fig. 3A**) in S/G2 cells, and it promotes HR.[45] HR is triggered when a 2-ended DSB is processed to a 3′ ssDNA tail via resection. Once the ssDNA is generated, it is rapidly bound by the RPA, which, in turn, facilitates Rad51 nucleofilament formation. The resultant Rad51 filament facilitates DNA strand invasion and exchange steps. The formation of RAD51 foci in response to IR represents an important step in the repair of DSBs.[46] As observed in a previous report,[47] we found that the number of Rad51 foci was significantly reduced in FANCD2$^{-/-}$ cells relative to FANCD2-WT cells post-treatment with Fe-particles radiation (**Fig. 3**). Collectively, this evidence clearly supports the notion that HR-mediated clustered DNA lesion repair is defective in FANCD2$^{-/-}$ cells due to defective DNA-end resection and Rad51 filament formation.

The mechanism by which FANCD2 participates in the processing of clustered DSBs is not clear. Recent findings indicate that an interaction between FANCD2 and CtIP is critical for DNA-end resection,[24,25] an important step in HR-mediated DSB repair. Additionally, a number of reports suggest that FANCD2 is involved in HR-mediated repair of DSBs.[29,45] Evidences show that DNA end-resection pathway is activated in response to clustered DSBs.[11,36] Further, reports support the idea that Rad51-mediated HR pathway is important for the repair of clustered DSBs.[10,48] Our data show that the number of RPA2 and Rad51 foci was significantly reduced in FANCD2$^{-/-}$ cells relative to FANCD2-WT cells (**Fig. 3**). Therefore, it is reasonable to assume that in the absence of FANCD2, DNA-end resection is affected. As a consequence, Rad51 recruitment is altered. Thus, HR-mediated clustered DSB repair is affected in FANCD2-deficient cells exposed to high-LET radiation.

FA pathway plays an important role in promoting HR during interstrand crosslink (ICL) repair, a loss FANCD2 increases sensitivity to agents that induce ICLs.[49] Though the extent of high-LET radiation induced ICL is not clear, it is highly possible that FANCD2 might be involved the processing of high-LET radiation induced ICLs. Further, co-localization of FANCD2 with γH2AX along the ionizing tracks traversed by Fe-particles (**Figure 1B**) clearly suggests that FANCD2 functions in clustered DSB repair. However, based on our current experimental strategy we can't distinguish the contribution of FANCD2 to high-LET radiation induced ICL and clustered DSB, and further experimental evidences are needed.

One important finding of our study is that the effect of Fe-particles radiation on replication fork progression, stalling, and new origin firing processes was more pronounced in FANCD2-deficient cells than in wild-type cells (**Fig. 5**). Evidences indicate that FA pathway members including FANCD2 protect nascent DNA stands at stalled replication forks from MRE11-mediated degradation.[26] Further, FANCD2 is shown to play roles in replication restart and suppression of new origin firing in response to replication stalling.[50] On the other hand, evidence suggests that DSBs inhibit replication fork elongation more effectively than base lesions or single-stranded breaks[51]; but, it is not clear why Fe-particles generated clustered DSBs cause a global effect on replication forks progression. However, it is reasonable to assume that in the absence of FANCD2, repair of clustered DSBs is affected, and as a consequence replication fork processes are altered in FANCD2-deficient cells in response to Fe-particles radiation. Future studies should reveal if and how high-LET radiation, in addition to complex DNA lesions, induces replication fork stalling and the precise functions of FA pathway in DNA replication and repair.

Our data clearly indicates that FANCD2 protects the genome in response to clustered DSBs. Our classical chromosome analysis revealed that the levels of chromosomal aberrations, including number of acentric fragments, were significantly elevated in Fe-particles irradiated FANCD2$^{-/-}$ cells relative to Fe-particles irradiated FANCD2-WT cells. The levels of chromosomal abnormalities were correlated with the extent of unrepaired DNA damage in these cells. Our study also suggests that FANCD2 is important for the proper segregation of chromosomes during anaphase. Reports suggest that mutations in HR repair factors cause defects in anaphase separation,[52] and the lagging chromosomes originate from acentric chromosome fragments.[53] Further, FANCD2-defective bone marrow cells exhibit cytokinesis failure.[54] Therefore, the acentric fragments could be passed to daughter cells by means of chromosome lagging and initiate the genomic instability. Additionally, elevated levels of anchorage-independent growth of irradiated FANCD2-deficient cells further support the occurrence of genomic instability. Thus, FANCD2 is important for the maintenance of genome stability in response to high-LET radiation.

In conclusion, we found that the repair of clustered DSBs is inefficient in FANCD2-deficient cells in the S/G2 phase of the cell cycle. This is mainly because of defective RPA2 and Rad51 recruitment to the sites of DSBs. In addition, replication fork processing is also defective in the absence of FANCD2. Consequently, FANCD2-deficient cells exhibit increased levels of gross-chromosomal aberrations, defective chromosome segregation and higher levels of anchorage-independent growth. Thus, the coordinated actions of FANCD2 in replication processes and clustered DSB repair are critical for cellular ability to protect genome in response to high-LET radiation.

Materials and Methods

Cell lines and culture conditions

The simian virus 40–transformed FANCD2-deficient (PD20) and the isogenic FANCD2-deficient cells complemented with wild-type FANCD2 (FANCD2-WT) were a kind gift from Dr. Alan D'Andrea (Harvard University, Cambridge, MA). FANCD2-WT and FANCD2$^{-/-}$ cells were grown in Dulbecco's modified Eagle medium (DMEM, Hyclone) supplemented with 10% fetal calf serum (FCS), 100 mg/ml streptomycin sulfate, 100 U/ml penicillin, and 1 mg/ml puromycin. HT1080 cells stably expressing EYFP-53BP1, mCherry-hCdt1, and AmCyan-hGeminin and U2OS cells stably expressing mCherry-Rad52, EYFP-53BP1, and AmCyan-hGeminin were grown in Minimum Essential Medium (MEM, Hyclone) supplemented with 10% FCS, 100 mg/ml streptomycin sulfate, and 100 U/ml penicillin. Cells were maintained at 37°C in a humidified 5% CO_2 incubator.

Irradiation

High-LET iron (Fe) particle beams were generated at the NASA Space Radiation Laboratory at Brookhaven National Laboratory, Long Island, NY. The energy of the Fe-particles used was 1 GeV/n and the dose rate ranged from 25 to 100 cGy/min. The LET of the Fe-particles was 150 keV/μm. The residual ranges of the beams were determined before each experiment and were used to calculate the track-averaged LET values.[55] To examine the recruitment of FANCD2 along the Fe-particle tracks, cells were irradiated horizontally (0° angle) and for all other experiments, cells were irradiated at 30° angle, as described in.[1]

For γ-irradiation, a ^{137}Cs γ-ray source was used. The dose rate was ~3.5 Gy/min. For all γ-irradiation and Fe-particles irradiation experiments, exponentially growing cells were irradiated at room temperature and then immediately transferred to a humidified 5% CO_2 incubator maintained at 37°C.

Antibodies

Anti-γH2AX mouse monoclonal antibody (Upstate Biotechnology), anti-RPA2 mouse monoclonal antibody (NA19L, EMD Millipore), anti-Rad51 rabbit polyclonal antibody (PC-130, Millipore), anti-BrdU mouse monoclonal antibody (347580, BD), anti-BrdU rat monoclonal antibody (NB500-169, Novus Biologicals), anti-FANCD2 polyclonal antibody (NB100-182, Novus Biologicals), anti-53BP1 polyclonal antibody (Cell Signaling), anti-Chk1 mouse monoclonal antibody (2360, Cell Signaling), anti-pChk1 (S317) rabbit polyclonal antibody (2344, Cell Signaling), anti-actin rabbit polyclonal antibody (A2055, Sigma), and anti-α-acetylated tubulin, (T6793, Sigma) were used. Fluorescent dye-conjugated secondary antibodies Alexa-488, Alexa-555, and Alexa-633 were purchased from Molecular Probes (Invitrogen).

Whole-cell and nuclear extract preparation and western blotting

Whole-cell extracts were prepared according to a published procedure.[56] Aliquots containing 50–100 μg protein were resolved by 6–10% SDS-PAGE, transferred onto nitrocellulose membrane, and reacted with indicated antibodies.[38]

Indirect immunostaining

Approximately 2×10^5 cells were seeded in a 6-well plate containing cover glasses, incubated for 48 hr, and then exposed to 1–2 Gy Fe-particles. Cells were fixed with 4% paraformaldehyde for 20 min at room temperature at different post-IR times and subjected to indirect immunofluorescence as described previously.[57] For the localization of RPA2 and RAD51, cells were washed 3 times in PBS and incubated in extraction buffer (10 mM HEPES, pH 7.4, 300 mM sucrose, 100 mM NaCl, 3 mM $MgCl_2$, 0.1% Triton X-100) on ice for 10 min prior to fixation. For immunostaining, cells were permeabilized in Triton X-100 (0.5% in PBS) on ice for 5 min, washed 3 times with PBS, incubated in blocking solution (5% goat serum in PBS) at room temperature for 60 min, and then incubated with primary antibodies (diluted in 5% goat serum) at room temperature for another 3 hr. Subsequently, cells were washed with 1% BSA in PBS, incubated with appropriate secondary antibodies (1:800 in 2.5% goat serum, 1% BSA, and PBS) at room temperature for 60 min, washed 5 times with 1% BSA, and mounted with mounting medium containing DAPI (Vectashield).

EdU-labeling

To detect S-phase cells, we used Click-iT^{TM} EdU Imaging Kit (Invitrogen, C10338). First, 2×10^5 cells were grown on cover glass for 24 hr, pulsed with 50 mM EdU for 30 min in growth medium, washed 3 times with 1 × PBS, and then exposed to Fe-particles in fresh medium. At different times after irradiation, cells were fixed with 4% PFA and immunostained with primary antibodies (anti-γH2AX) as described in the indirect immunostaining section. After primary antibody incubation, cells were washed 3 times with 1% BSA and incubated with EdU Click-iT^{TM} kit cocktail mixture for 30 min at room temperature according to manufacturer's instructions. Subsequently, cells were washed 3 times with 1% BSA and incubated with appropriate Alexa fluor conjugated secondary antibodies diluted in 1% BSA and 2.5% goat serum for 1 hr. Cover glasses were washed 5 times with 1% BSA for 5 min each, and the nuclei were counterstained with DAPI.

Image acquisition and foci dissolution kinetics assay

Images were captured using a LSM 510 Meta laser scanning confocal microscope with a 63 × 1.4 NA Plan-Apochromat oil immersion objective. Images were taken at z-sections (15–20 sections) of 0.35-μm intervals using the 488-nm (Alexa 488), 543-nm (rhodamine/Alexa 555), 633-nm (Alexa 633), and 405-nm (for DAPI) lasers. The tube current of the 488-nm argon laser was set at 6.1 A. The laser intensity was typically set to 3–5% transmission of the maximum intensity with the pinhole opened between 1 (for foci) and 2 (for nuclei) Airy units. For RPA2, RAD51, and γH2AX foci counting, the z-sections were assembled using the Imaris software and the foci number were enumerated using the spot detection function of the Imaris software. Quantification of foci was done from images of 100–200 cells for each time point from 2 to 3 independent experiments.[57]

BrdU labeling and flow cytometry

Exponentially growing cells were pulsed with 30 μM BrdU for 30 min in growth medium just before irradiation. Cells were washed 3 times with 1 × PBS and exposed to Fe-particles in fresh culture medium. Following irradiation, cells were washed twice in 1 × PBS and fixed with ice-cold 70% ethanol at –20°C overnight. For BrdU flow cytometry, cells were first washed twice with cold 1 × PBS and then treated with 100 mg/mL RNase containing 5% Tween-20 in 1 × PBS at 37°C for 30 min. To denature DNA, cells were resuspended in ~2 M HCl (1 mL per 10^6 cells) containing 0.5% Tween-20, incubated at 37°C for 30 min, and then neutralized by washing twice with 1 × PBS. Following neutralization, cells were incubated in 100 μl of 1 × PBS containing 0.1% Tween-20, 1% BSA, and anti-BrdU conjugated with FITC (1:100; Molecular Probes, B35130) at room temperature for 2 hr. After washing with 1% BSA, cells were stained with 10 mg/mL propidium iodide (Sigma) at room temperature for 30 min. Subsequently, cells were filtered with nylon mesh and subjected to flow cytometry (FACScan, Becton Dickinson). The data were analyzed using FlowJo software.

Phospho-histone 3 (pH3) detection

To quantity mitotic cells at different times after Fe-particles or γ irradiation, cells were washed twice in 1 × PBS and fixed with ice-cold 70% ethanol at –20°C overnight. Cells were first washed twice with ice-cold 1 × PBS, permeabilized in Triton X-100 (0.25%; Sigma) on ice for 5 min, incubated in blocking solution (5% goat serum in PBS) at room temperature for 60 min, and

then incubated with anit-pH3 rabbit polyclonal antibodies (1:250; Millipore 06–570) in 5% goat serum (Jackson Immuno Research, 005-000-121) at room temperature for another 2 hr. Subsequently, cells were washed with 1% BSA in 1 × PBS, incubated with secondary goat anti-rabbit 488 antibody (1:100, Invitrogen A11008), diluted in 2.5% goat serum, 1% BSA, and PBS at room temperature for 30 min, washed twice with 1% BSA, and subjected to flow cytometry (FACScan, Becton Dickinson).

DNA fiber assay

DNA fiber assay was carried out as described previously.[38] Briefly, 2.5×10^5 and 1×10^6 cells were plated in a 6-well plate (labeled) and 10-cm dishes (unlabeled), respectively, and incubated for 24 hr. Cells in 6-well plates were first labeled with IdU (150 mM, 50-90-8, Sigma) for 30 min, washed 4 times with warm PBS, exposed to 1 Gy of Fe ions and then labeled with CldU (150 mM, I7125, Sigma) for 30 min. After three washes with warm PBS, both labeled and unlabeled cells were trypsinized and counted. Cell numbers were adjusted to a final concentration of 10^6/ml and mixed at 1:15 ratio (labeled:unlabeled) and lysed on a clean glass slide in 20 μl of lysis buffer (0.5% SDS, 50 mM EDTA and 200 mM Tris-HCl pH7.4) for 8 min. The slides were tilted slightly (15° angle) to help DNA spread slowly. After air drying the samples, DNA on the glass slide was fixed with methanol:acetic acid (3:1) at room temperature for 8–10 min and air-dried. Slides were stored in 70% ethanol at 4°C until use. For the immunostaining of DNA fibers, slides were first washed 3 times with PBS at room temperature. To denature DNA, slides were incubated in 2.5 N HCl in a glass jar at 37°C for 50 min and then neutralized by washing 4 times with PBS. Following neutralization, slides were incubated in 5% goat serum in PBS for 2 hr at room temperature. Subsequently, mouse anti-BrdU antibody (BD, 347580) and rat anti-BrdU antibody (Novus Biologicals, NB500-169) were diluted in 5% goat serum, 0.1% Triton X100, and PBS. Slides were incubated with antibody at 37°C for 1 hr in a humidified chamber, washed 3 times in PBS containing 0.1% TritonX100, and incubated with anti-rat Alexa 488 and anti-mouse Alexa 555 antibodies in 5% goat serum and 0.1% Triton X-100 for an additional 1 hr. After washing 3 times with PBS containing 0.1% TritionX-100, slides were mounted in mounting medium without DAPI (Vectashield). Images were acquired using a fluorescent microscope (Zeiss) and the DNA fiber lengths were measured using AxioVision Ver 4.8 software. More than 100–200 fibers per sample from 2–3 independent experiments were used for the measurement. During IdU and CldU labeling, cells were maintained at 37°C in a humidified 5% CO_2 incubator.

Cell survival assay

Cell survival was measured using a colony formation assay.[58] For γ-irradiation, various numbers of cells (~2×10^2 to 3×10^3) were plated in triplicate and incubated for 6–8 hr. Then cells were irradiated with graded doses (0, 2, 4, 6, 8 Gy) of γ−rays and allowed to form colonies for 9 days. For Fe-particle exposure, cells were seeded in T-25 flasks, incubated for 24 hr prior to irradiation, and irradiated vertically with doses of 0, 0.25, 0.5, 1, 1.5, and 2 Gy. Immediately after irradiation, different number of cells (2×10^2 to 3×10^3) were plated in 60-mm dishes in triplicate and incubated for 9 days. Colonies were washed once with 1 × PBS, fixed with 70% ethanol for 10 min, then stained with 0.5% crystal violet dissolved in 1 × PBS, and the colonies were counted. Survival curves were generated from 4 independent experiments with colony numbers normalized to sham-treated controls.

Chromosome aberrations

Chromosome aberrations were detected as described previously.[1] Briefly, 16 hr after irradiation, chromosome preparations were made by accumulating metaphases in the presence of 0.1 mg/mL colcemid (Irvine Scientific) for 5 hr. Cells were trypsinized and then washed once with PBS and incubated in 10 mL of hypotonic solution (0.075 M KCl) at 37°C for 13 min. Cells were pre-fixed with 1/10 volume of ice-cold methanol:acetic acid (3:1 ratio) in hypotonic solution and then centrifuged at 1000 × g for 5 min at 4°C. Subsequently, the cells were fixed with methanol: acetic acid (3:1 ratio) on ice for 30 min and kept at −20°C until use. Cells were dropped onto pre-cleaned cover slides, stained with 5% Giemsa (GIBCO, 10092-013) for 4 min at room temperature, and then washed with dH_2O. Images were taken using an Olympus microscope (100 × objective) equipped with an Image Spot camera (Spot Imaging Solutions), and chromosome aberrations were scored as previously described.[1]

Anaphase bridge detection

Approximately 5×10^4 cells were seeded on cover glasses and cultured for 48 hr. Cells were exposed to 1 Gy of Fe-particles, fixed with 4% PFA at 72 hr after IR, and then immunostained with anti-α-acetylated tubulin (Sigma, 1:2000, T6793). Lagging chromosomes or chromatin bridges were identified as the blue DAPI fluorescent-positive materials observed in the mid-zone or continuously along the segregation track in anaphase or telophase, respectively.[53] The frequency of cells with chromatin bridges or lagging chromosomes was scored. At least 100 anaphase or telophase images were acquired using a fluorescent microscope (Zeiss). Two independent experiments were performed.

Soft-agar colony formation assay

An anchorage-independent soft-agar colony formation assay was carried out to assess the impact of Fe-particle irradiation on cellular transformation. For this purpose, FANCD2-WT cells were irradiated with 2 Gy Fe-particles and cultured for 14 days. Subsequently, approximately 1.5×10^5 cells were suspended in growth medium containing 0.3% low melting agarose (Fisher Scientific), and plated onto solidified 0.6% agarose in growth medium in a 100-mm cell culture dish. Growth medium was changed once a week and cells were allowed to form colonies for 45 days at 37°C under 5% CO_2. At the end of the incubation, dishes were washed once with 1 × PBS and stained with 1 mg/ml iodonitrotetrazolium violet (Sigma) overnight at 37°C.

Dishes were then washed once with 1 × PBS and visible colonies bigger than 0.1 mm in diameter in the entire dish were counted under a Carl Zeiss Stereo Microscope.[59] Each sample were plated in triplicate, 7 repeats from 2 independent experiments were performed.

Statistical analyses

Data are expressed as means ±SEM or STDEV of at least 2 independent experiments. The Student's t test was performed to calculate the level of significance and a value of $P < 0.05$ was considered statistically significant.

Disclosure of Potential Conflicts of Interest

No potential conflicts of interest were disclosed.

Acknowledgments

We are thankful to all the members of the NSRL facility at Brookhaven National laboratory for their help in Fe-particles irradiation. We thank Dr. Alan D'Andrea for FANCD2$^{-/-}$ (P20) and FANCD2$^{-/-}$ cells complemented with FANCD2 and Dr. Atsushi Miyawaki for FUCCI plasmids.

Funding

This work was supported by the National Aeronautics and Space Association grants NNX13AD57G (AA) and NNX11AC54G (AA).

Supplemental Material

Supplemental data for this article can be accessed on the publisher's website.

References

1. Asaithamby A, Hu B, Chen DJ. Unrepaired clustered DNA lesions induce chromosome breakage in human cells. Proc Natl Acad Sci U S A 2011; 108:8293-8; PMID:21527720; http://dx.doi.org/10.1073/pnas.1016045108
2. Goodhead DT, Thacker J, Cox R. Weiss Lecture. Effects of radiations of different qualities on cells: molecular mechanisms of damage and repair. Int J Radiat Biol 1993; 63:543-56; PMID:8099101; http://dx.doi.org/10.1080/09553009314450721
3. Sutherland BM, Bennett PV, Sidorkina O, Laval J. Clustered DNA damages induced in isolated DNA and in human cells by low doses of ionizing radiation. Proc Natl Acad Sci U S A 2000; 97:103-8; PMID:10618378; http://dx.doi.org/10.1073/pnas.97.1.103
4. Brenner DJ, Ward JF. Constraints on energy deposition and target size of multiply damaged sites associated with DNA double-strand breaks. Int J Radiat Biol 1992; 61:737-48; PMID:1351522; http://dx.doi.org/10.1080/09553009214551591
5. Blaisdell JO, Harrison L, Wallace SS. Base excision repair processing of radiation-induced clustered DNA lesions. Radiat Prot Dosimetry 2001; 97:25-31; PMID:11763354; http://dx.doi.org/10.1093/oxfordjournals.rpd.a006634
6. Harrison L, Hatahet Z, Purmal AA, Wallace SS. Multiply damaged sites in DNA: interactions with Escherichia coli endonucleases III and VIII. Nucleic Acids Res 1998; 26:932-41; PMID:9461450; http://dx.doi.org/10.1093/nar/26.4.932
7. Nikjoo H, O'Neill P, Wilson WE, Goodhead DT. Computational approach for determining the spectrum of DNA damage induced by ionizing radiation. Radiat Res 2001; 156:577-83; PMID:11604075; http://dx.doi.org/10.1667/0033-7587(2001)156%5b0577:CAFDTS%5d2.0.CO;2
8. Wang H, Wang X, Zhang P, Wang Y. The Ku-dependent non-homologous end-joining but not other repair pathway is inhibited by high linear energy transfer ionizing radiation. DNA Repair (Amst) 2008; 7:725-33; PMID:18325854; http://dx.doi.org/10.1016/j.dnarep.2008.01.010
9. Wang J, Pluth JM, Cooper PK, Cowan MJ, Chen DJ, Yannone SM. Artemis deficiency confers a DNA double-strand break repair defect and Artemis phosphorylation status is altered by DNA damage and cell cycle progression. DNA Repair 2005; 4:556-70; PMID:15811628; http://dx.doi.org/10.1016/j.dnarep.2005.02.001
10. Zafar F, Seidler SB, Kronenberg A, Schild D, Wiese C. Homologous recombination contributes to the repair of DNA double-strand breaks induced by high-energy iron ions. Radiat Res 2010; 173:27-39; PMID:20041757; http://dx.doi.org/10.1667/RR1910.1
11. Yajima H, Fujisawa H, Nakajima NI, Hirakawa H, Jeggo PA, Okayasu R, Fujimori A. The complexity of DNA double strand breaks is a critical factor enhancing end-resection. DNA Repair 2013; 12:936-46; PMID:24041488; http://dx.doi.org/10.1016/j.dnarep.2013.08.009
12. Fanconi G. Familial constitutional panmyelocytopathy, Fanconi's anemia (F.A.). I. Clinical aspects. Semin Hematol 1967; 4:233-40; PMID:6074578
13. Kee Y, D'Andrea AD. Expanded roles of the Fanconi anemia pathway in preserving genomic stability. Genes Dev 2010; 24:1680-94; PMID:20713514; http://dx.doi.org/10.1101/gad.1955310
14. Moldovan GL, D'Andrea AD. How the fanconi anemia pathway guards the genome. Annu Rev Genet 2009; 43:223-49; PMID:19686080; http://dx.doi.org/10.1146/annurev-genet-102108-134222
15. Crossan GP, Patel KJ. The Fanconi anaemia pathway orchestrates incisions at sites of crosslinked DNA. J Pathol 2012; 226:326-37; PMID:21956823; http://dx.doi.org/10.1002/path.3002
16. Kottemann MC, Smogorzewska A. Fanconi anaemia and the repair of Watson and Crick DNA crosslinks. Nature 2013; 493:356-63; PMID:23325218; http://dx.doi.org/10.1038/nature11863
17. Garcia-Higuera I, Taniguchi T, Ganesan S, Meyn MS, Timmers C, Hejna J, Grompe M, D'Andrea AD. Interaction of the Fanconi anemia proteins and BRCA1 in a common pathway. Mol Cell 2001; 7:249-62; PMID:11239454; http://dx.doi.org/10.1016/S1097-2765(01)00173-3
18. Smogorzewska A, Matsuoka S, Vinciguerra P, McDonald ER 3rd, Hurov KE, Luo J, Ballif BA, Gygi SP, Hofmann K, D'Andrea AD, et al. Identification of the FANCI protein, a monoubiquitinated FANCD2 paralog required for DNA repair. Cell 2007; 129:289-301; PMID:17412408; http://dx.doi.org/10.1016/j.cell.2007.03.009
19. Bunting SF, Nussenzweig A. Dangerous liaisons: Fanconi anemia and toxic nonhomologous end joining in DNA crosslink repair. Mol Cell 2010; 39:164-6; PMID:20670885; http://dx.doi.org/10.1016/j.molcel.2010.07.016
20. Shen C, Houghton PJ. Targeting FANCD2 for therapy sensitization. Oncotarget 2014; 5:3426-7; PMID:24913333
21. Patil AA, Sayal P, Depondt ML, Beveridge RD, Roylance A, Kriplani DH, Myers KN, Cox A, Jellinek D, Fernando M, et al. FANCD2 re-expression is associated with glioma grade and chemical inhibition of the Fanconi Anaemia pathway sensitises gliomas to chemotherapeutic agents. Oncotarget 2014; 5:6414-24; PMID:25071006
22. Taniguchi T, Garcia-Higuera I, Andreassen PR, Gregory RC, Grompe M, D'Andrea AD. S-phase-specific interaction of the Fanconi anemia protein, FANCD2, with BRCA1 and RAD51. Blood 2002; 100:2414-20; PMID:12239151; http://dx.doi.org/10.1182/blood-2002-01-0278
23. Panneerselvam J, Pickering A, Han B, Li L, Zheng J, Zhang J, Zhang Y, Fei P. Basal level of FANCD2 monoubiquitination is required for the maintenance of a sufficient number of licensed-replication origins to fire at a normal rate. Oncotarget 2014; 5:1326-37; PMID:24658369
24. Unno J, Itaya A, Taoka M, Sato K, Tomida J, Sakai W, Sugasawa K, Ishiai M, Ikura T, Isobe T, et al. FANCD2 binds CtIP and regulates DNA-end resection during DNA interstrand crosslink repair. Cell Rep 2014; 7:1039-47; PMID:24794430; http://dx.doi.org/10.1016/j.celrep.2014.04.005
25. Murina O, von Aesch C, Karakus U, Ferretti LP, Bolck HA, Hanggi K, Sartori AA. FANCD2 and CtIP cooperate to repair DNA interstrand crosslinks. Cell Rep 2014; 7:1030-8; PMID:24794434; http://dx.doi.org/10.1016/j.celrep.2014.03.069
26. Schlacher K, Wu H, Jasin M. A distinct replication fork protection pathway connects Fanconi anemia tumor suppressors to RAD51-BRCA1/2. Cancer Cell 2012; 22:106-16; PMID:22789542; http://dx.doi.org/10.1016/j.ccr.2012.05.015
27. Pichierri P, Rosselli F. The DNA crosslink-induced S-phase checkpoint depends on ATR-CHK1 and ATR-NBS1-FANCD2 pathways. EMBO J 2004; 23:1178-87; PMID:14988723; http://dx.doi.org/10.1038/sj.emboj.7600113
28. Mechali M, Lutzmann M. The cell cycle: now live and in color. Cell 2008; 132:341-3; PMID:18267067; http://dx.doi.org/10.1016/j.cell.2008.01.031
29. Taniguchi T, Garcia-Higuera I, Xu B, Andreassen PR, Gregory RC, Kim ST, Lane WS, Kastan MB, D'Andrea AD. Convergence of the fanconi anemia and ataxia telangiectasia signaling pathways. Cell 2002; 109:459-72; PMID:12086603; http://dx.doi.org/10.1016/S0092-8674(02)00747-X
30. Wang X, Andreassen PR, D'Andrea AD. Functional interaction of monoubiquitinated FANCD2 and BRCA2/FANCD1 in chromatin. Mol Cell Biol 2004; 24:5850-62; PMID:15199141; http://dx.doi.org/10.1128/MCB.24.13.5850-5862.2004
31. Yamamoto K, Hirano S, Ishiai M, Morishima K, Kitao H, Namikoshi K, Kimura M, Matsushita N, Arakawa H, Buerstedde JM, et al. Fanconi anemia protein FANCD2 promotes immunoglobulin gene conversion and DNA repair through a mechanism related to

homologous recombination. Mol Cell Biol 2005; 25:34-43; PMID:15601828; http://dx.doi.org/10.1128/MCB.25.1.34-43.2005
32. Seki S, Ohzeki M, Uchida A, Hirano S, Matsushita N, Kitao H, Oda T, Yamashita T, Kashihara N, Tsubahara A, et al. A requirement of FancL and FancD2 monoubiquitination in DNA repair. GenesCells 2007; 12:299-310; http://dx.doi.org/10.1111/j.1365-2443.2007.01054.x
33. Lok BH, Powell SN. Molecular pathways: understanding the role of Rad52 in homologous recombination for therapeutic advancement. Clin Cancer Res 2012; 18:6400-6; PMID:23071261; http://dx.doi.org/10.1158/1078-0432.CCR-11-3150
34. Plate I, Hallwyl SC, Shi I, Krejci L, Muller C, Albertsen L, Sung P, Mortensen UH. Interaction with RPA is necessary for Rad52 repair center formation and for its mediator activity. J Biol Chemis 2008; 283:29077-85; PMID:18703507; http://dx.doi.org/10.1074/jbc.M804881200
35. Chapman JR, Taylor MR, Boulton SJ. Playing the end game: DNA double-strand break repair pathway choice. Mol Cell 2012; 47:497-510; PMID:22920291; http://dx.doi.org/10.1016/j.molcel.2012.07.029
36. Averbeck NB, Ringel O, Herrlitz M, Jakob B, Durante M, Taucher-Scholz G. DNA end resection is needed for the repair of complex lesions in G1-phase human cells. Cell Cycle 2014; 13:2509-16; PMID:25486192; http://dx.doi.org/10.4161/15384101.2015.941743
37. Lossaint G, Larroque M, Ribeyre C, Bec N, Larroque C, Decaillet C, Gari K, Constantinou A. FANCD2 binds MCM proteins and controls replisome function upon activation of s phase checkpoint signaling. Mol Cell 2013; 51:678-90; PMID:23993743; http://dx.doi.org/10.1016/j.molcel.2013.07.023
38. Su F, Mukherjee S, Yang Y, Mori E, Bhattacharya S, Kobayashi J, Yannone SM, Chen DJ, Asaithamby A. Nonenzymatic role for WRN in preserving nascent DNA strands after replication stress. Cell Rep 2014; 9:1387-401; PMID:25456133; http://dx.doi.org/10.1016/j.celrep.2014.10.025
39. Montgomery E, Wilentz RE, Argani P, Fisher C, Hruban RH, Kern SE, Lengauer C. Analysis of anaphase figures in routine histologic sections distinguishes chromosomally unstable from chromosomally stable malignancies. Cancer Biol Ther 2003; 2:248-52; PMID:12878857; http://dx.doi.org/10.4161/cbt.2.3.362
40. Hoffelder DR, Luo L, Burke NA, Watkins SC, Gollin SM, Saunders WS. Resolution of anaphase bridges in cancer cells. Chromosoma 2004; 112:389-97; PMID:15156327; http://dx.doi.org/10.1007/s00412-004-0284-6
41. Rosefort C, Fauth E, Zankl H. Micronuclei induced by aneugens and clastogens in mononucleate and binucleate cells using the cytokinesis block assay. Mutagenesis 2004; 19:277-84; PMID:15215326; http://dx.doi.org/10.1093/mutage/geh028
42. Hu L, Filippakis H, Huang H, Yen TJ, Gjoerup OV. Replication stress and mitotic dysfunction in cells expressing simian virus 40 large T antigen. J Virol 2013; 87:13179-92; PMID:24067972; http://dx.doi.org/10.1128/JVI.02224-13
43. Piperno G, LeDizet M, Chang XJ. Microtubules containing acetylated alpha-tubulin in mammalian cells in culture. J Cell Biol 1987; 104:289-302; PMID:2879846; http://dx.doi.org/10.1083/jcb.104.2.289
44. Wang H, Zhang X, Wang P, Yu X, Essers J, Chen D, Kanaar R, Takeda S, Wang Y. Characteristics of DNA-binding proteins determine the biological sensitivity to high-linear energy transfer radiation. Nucleic Acids Res 2010; 38:3245-51; PMID:20150414; http://dx.doi.org/10.1093/nar/gkq069
45. Nakanishi K, Yang YG, Pierce AJ, Taniguchi T, Digweed M, D'Andrea AD, Wang ZQ, Jasin M. Human Fanconi anemia monoubiquitination pathway promotes homologous DNA repair. Proc Natl Acad Sci U S A 2005; 102:1110-5; PMID:15650050; http://dx.doi.org/10.1073/pnas.0407796102
46. Tarsounas M, Davies D, West SC. BRCA2-dependent and independent formation of RAD51 nuclear foci. Oncogene 2003; 22:1115-23; PMID:12606939; http://dx.doi.org/10.1038/sj.onc.1206263
47. Digweed M, Rothe S, Demuth I, Scholz R, Schindler D, Stumm M, Grompe M, Jordan A, Sperling K. Attenuation of the formation of DNA-repair foci containing RAD51 in Fanconi anaemia. Carcinogenesis 2002; 23:1121-6; PMID:12117768; http://dx.doi.org/10.1093/carcin/23.7.1121
48. Asaithamby A, Chen DJ. Mechanism of cluster DNA damage repair in response to high-atomic number and energy particles radiation. Mutat Res 2011; 711:87-99; PMID:21126526; http://dx.doi.org/10.1016/j.mrfmmm.2010.11.002
49. Kim H, D'Andrea AD. Regulation of DNA cross-link repair by the Fanconi anemia/BRCA pathway. Genes Dev 2012; 26:1393-408; PMID:22751496; http://dx.doi.org/10.1101/gad.195248.112
50. Yeo JE, Lee EH, Hendrickson EA, Sobeck A. CtIP mediates replication fork recovery in a FANCD2-regulated manner. Hum Mol Genet 2014; 23:3695-705; PMID:24556218; http://dx.doi.org/10.1093/hmg/ddu078
51. Parplys AC, Petermann E, Petersen C, Dikomey E, Borgmann K. DNA damage by X-rays and their impact on replication processes. Radiother Oncol 2012; 102:466-71; PMID:22326574; http://dx.doi.org/10.1016/j.radonc.2012.01.005
52. Laulier C, Cheng A, Stark JM. The relative efficiency of homology-directed repair has distinct effects on proper anaphase chromosome separation. Nucleic Acids Res 2011; 39:5935-44; PMID:21459848; http://dx.doi.org/10.1093/nar/gkr187
53. Huang Y, Hou H, Yi Q, Zhang Y, Chen D, Jiang E, Xia Y, Fenech M, Shi Q. The fate of micronucleated cells post X-irradiation detected by live cell imaging. DNA Repair 2011; 10:629-38; PMID:21543268; http://dx.doi.org/10.1016/j.dnarep.2011.04.010
54. Vinciguerra P, Godinho SA, Parmar K, Pellman D, D'Andrea AD. Cytokinesis failure occurs in Fanconi anemia pathway-deficient murine and human bone marrow hematopoietic cells. J Clin Invest 2010; 120:3834-42; PMID:20921626; http://dx.doi.org/10.1172/JCI43391
55. Asaithamby A, Hu B, Delgado O, Ding LH, Story MD, Minna JD, Shay JW, Chen DJ. Irreparable complex DNA double-strand breaks induce chromosome breakage in organotypic three-dimensional human lung epithelial cell culture. Nucleic Acids Res 2011; 39:5474-88; PMID:21421565; http://dx.doi.org/10.1093/nar/gkr149
56. Puente BN, Kimura W, Muralidhar SA, Moon J, Amatruda JF, Phelps KL, Grinsfelder D, Rothermel BA, Chen R, Garcia JA, et al. The oxygen-rich postnatal environment induces cardiomyocyte cell-cycle arrest through DNA damage response. Cell 2014; 157:565-79; PMID:24766806; http://dx.doi.org/10.1016/j.cell.2014.03.032
57. Asaithamby A, Chen DJ. Cellular responses to DNA double-strand breaks after low-dose gamma-irradiation. Nucleic Acids Res 2009; 37:3912-23; PMID:19401436; http://dx.doi.org/10.1093/nar/gkp237
58. Asaithamby A, Uematsu N, Chatterjee A, Story MD, Burma S, Chen DJ. Repair of HZE-particle-induced DNA double-strand breaks in normal human fibroblasts. Radiat Res 2008; 169:437-46; PMID:18363429; http://dx.doi.org/10.1667/RR1165.1
59. Suzuki F, Suzuki K, Nikaido O. An improved soft agar method for determining neoplastic transformation in vitro. J Tissue Culture Methods 1983; 8:109-13; http://dx.doi.org/10.1007/BF01842703